

Transition to Super uid Turbulence

V . B . E ltsov ^y, M . K rusius , and G . E . Volovik ^z

Low Tem perature Laboratory, Helsinki University of Technology
P . O . Box 2200, FIN -02015 HUT, Finland

^yK apitza Institute of Physical Problems, Kosygina 2, 119334 Moscow, Russia

^zLandau Institute for Theoretical Physics, Kosygina 2, 119334 Moscow, Russia

Turbulence in super uids depends crucially on the dissipative damping in vortex motion. This is observed in the B phase of super uid ^3He where the dynamics of quantized vortices changes radically in character as a function of temperature. An abrupt transition to turbulence is the most peculiar consequence. As distinct from viscous hydrodynamics, this transition to turbulence is not governed by the velocity-dependent Reynolds number, but by a velocity-independent dimensionless parameter $1=q$ which depends only on the temperature-dependent mutual friction $\{\$ the dissipation which sets in when vortices move with respect to the normal excitations of the liquid. At large friction and small values of $1=q \ll 1$ the dynamics is vortex number conserving, while at low friction and large $1=q \gg 1$ vortices are easily destabilized and proliferate in number. A new measuring technique was employed to identify this hydrodynamic transition: the injection of a tight bundle of many small vortex loops in applied vortex-free flow at relatively high velocities. These vortices are ejected from a vortex sheet covering the AB interface when a two-phase sample of $^3\text{He-A}$ and $^3\text{He-B}$ is set in rotation and the interface becomes unstable at a critical rotation velocity, triggered by the super uid Kelvin-Helmholtz instability.

PACS numbers: 47.37, 67.40, 67.57

1. INTRODUCTION

Super uid turbulence $\{\$ the tangled motion of quantized vortex lines in super uid $^4\text{He-II}$ $\{\$ has been known to exist for fifty years¹. By increasing the applied flow velocity beyond some relatively low critical value, at which vortices become mobile, their turbulent motion is started and super uid flow becomes dissipative². In this context we mean with applied flow the

counter flow velocity $v = v_n - v_s$, the difference between the velocities v_n of the normal and v_s of the superfluid components, which is created by external means.

Only recently it has been realized from measurements on superfluid $^3\text{He-B}$ that turbulence is not necessarily a generic property of all superfluids, but one whose presence crucially depends on the damping in vortex motion.³ The damping, or more accurately the mutual friction dissipation, turns out to govern the onset of turbulence, dividing vortex motion in $^3\text{He-B}$ to superconductor-like regular behavior at high temperatures, where the vortex number is conserved in dynamic processes, and to ^4He -like disordered behavior at low temperatures, where turbulence easily sets in when perturbations are introduced in superfluid flow.

The transition to turbulence in superfluids can be compared to that in viscous flow, as discussed in Ref. [4] on linear pipe flow with circular cross section. Here the transition is governed by the velocity-dependent Reynolds number $Re = UD/\nu$, where U is the mean velocity, D the characteristic length scale (the pipe diameter in Ref. [4]), and ν the kinematic viscosity. In the 16m long circular pipe of Ref. [4] laminar flow is stable at flow velocities $Re < 20\,000$. However, on injecting a controlled square pulse of perturbing flow azimuthally in the linear stream, the flow can be converted from laminar to turbulent over some length of the pipe. This turbulence travels downstream in the pipe, while upstream in the absence of the perturbation laminar flow again recovers. The critical amplitude of the perturbing mass flux u_{inj} , required to reach the transient turbulent state, was found to obey a scaling law of the form $u_{inj} = u_{pipe} Re^\alpha$, where the exponent has the value $\alpha = 1.0 \pm 0.01$.

To generate the transition to turbulence in superfluids, one or several vortices are injected in rotating vortex-free flow of $^3\text{He-B}$.⁵ It is then found that the transition is not governed by viscosity (which is absent for the superfluid fraction of the liquid), but by the mutual friction between vortices and the normal fraction of the liquid. As distinct from viscosity, which enters the Reynolds number as the dimensional kinematic viscosity $\nu = \eta/\rho$, mutual friction is described by two dimensionless parameters which represent its dissipative and reactive components. In $^3\text{He-B}$ in the range of the transition to turbulence both parameters are of comparable magnitude and have to be taken into account. In $^4\text{He-II}$ the reactive mutual friction parameter is much smaller and is usually neglected (see review [6]). In the superfluid, the viscosity dependent Reynolds number has to be replaced by a dimensionless characteristic number which is called $1=q$ and only depends on the two mutual friction parameters. In particular as opposed to Reynolds number, $1=q$ is velocity independent which is also observed in measurement

Transition to Superfluid Turbulence

at higher flow velocities as the limiting case. In this short review we focus on this limiting regime, which corresponds to the case when a sufficient number of closely spaced seed vortex loops is injected, so that they immediately start interacting and instantaneously produce turbulence.³

If the number of seed vortices is reduced or their spacing is increased, then the flow perturbation is weakened and the transition to turbulence moves to higher values of $l=q$. In this case more new vortices need to be generated, before they can start interacting turbulently. Measurements with injection down to the limit of one single seed vortex are discussed in Refs. [7,8]. Obviously such cases require some additional mechanism, which leads to an increase in the number of vortices in the low-density regime, when vortices do not yet interact. This is the single vortex instability in applied flow which via loop formation and reconnection generates new independent vortices. In this way the transition to turbulence becomes a complex process of series coupled mechanisms in the regime of small flow perturbation.⁹ However, independently of the applied perturbation, in all these measurements the onset of turbulence is displayed as an abrupt transition, which takes place within a narrow distribution of $l=q$ values. Moreover, the average of this distribution of $l=q$ values proves to depend on the magnitude of the applied perturbation in a power-law manner.

Comparing measurements on the transition to turbulence in viscous and superfluid flow, we notice that they proceed in somewhat different manner. Nevertheless, there are similarities: In both cases (i) the initial state is perturbed externally by means of a quantitatively controlled disturbance which (ii) sets off turbulence for a short length of time if (iii) the perturbation is of sufficient amplitude, with power-law dependence on the relevant controlling parameter (which is Re in viscous flow and the mutual friction dependent parameter $l=q$ in superfluids).

There are special reasons why the transition to turbulence as a function of mutual friction has not been observed in superfluid 4He -II and was only recently discovered in superfluid 3He -B. As distinct from 4He -II, 3He -B is a Fermi superfluid, where the superfluidity is caused by Cooper pairing. The mutual friction between vortices and the normal fraction of the liquid, which is composed of fermionic quasiparticles, is mediated by quasiparticles populating the vortex core states,¹⁰ the so-called fermion zero modes¹¹. The scattering between the two types of quasiparticles leads to mutual friction and is described by a theory similar to the BCS theory of superconductivity. As a result the parameter $q(T)$ appears to be a dimensionless function of the dimensionless parameter $T=T_c$. In Fermi superfluids in the weak coupling approximation this parameter crosses unity at $T \approx 0.6T_c$, i.e. in the middle of the experimentally accessible temperature range of 3He -B. (In the cold

superfluid fermionic gases discussed in Ref. [12] q can be adjusted with a magnetic field if the system is close to the Feshbach resonance.)

In contrast, in the boson superfluid $^4\text{He-II}$ vortex dynamics is practically always in the turbulent regime (see review [6]). Regular flow of vortices could be perhaps expected only within microkelvins from the superfluid transition temperature T_λ , but there is not yet enough information on vortex dynamics in this regime. Even there, the low viscosity of the normal component (in $^4\text{He-II}$ the normal component is one of the least viscous fluids existing) causes its flow to become easily turbulent, which can in turn influence the flow of the superfluid component. In contrast, in $^3\text{He-B}$ the normal component has 10^4 times higher oil-like viscosity and is practically always in a state of laminar flow. The absence of turbulence in the flow of the normal component of $^3\text{He-B}$ amounts to a considerable simplification and leads to new effects, which are absent in $^4\text{He-II}$. An example is a new scaling law for the Kolmogorov-Richardson cascade in developed homogeneous superfluid turbulence.^{13,14}

The injection mechanism, which led to the discovery of the transition to turbulence as a function of $l=q$, is of particular interest. Here the injected seed vortices originate from the AB interface in a two-phase sample of $^3\text{He-A}$ and $^3\text{He-B}$. The seed vortices are tossed as a tight bundle of some 10 loops across the AB interface from $^3\text{He-A}$ into the vortex-free flow of $^3\text{He-B}$. This happens when the interface becomes unstable with respect to wave formation at a well-defined critical value for superfluid counterflow parallel to the interface. During the non-linear stage of this corrugation instability, the vortices in the deepest corrugation of the interface wave are ejected on the B-phase side of the interface. The instability itself, known as the superfluid Kelvin-Helmholtz shear flow instability, is reproducible and predictable, its measurements and theory match without fitting parameters. This is different from the ordinary Kelvin-Helmholtz instability at the interface between two viscous liquids or gases. In viscous fluids the initial state is not well described, since the shear-flow configuration is not an equilibrium situation and cannot be expressed as a solution of the Navier-Stokes equation. Interestingly, the superfluid Kelvin-Helmholtz instability shares some characteristics with the instability of quantum vacuum within the horizon or ergoregion of the black hole.¹⁵

In this short review¹⁶ we shall first introduce the superfluid Kelvin-Helmholtz instability and the injection of vortex seed loops in Sec. 2. Then follows in Sec. 3 a description of the transition to turbulence in the case when turbulence is instantaneously started by the injected vortex loops.

2. SUPERFLUID KELVIN-HELMHOLTZ INSTABILITY

Transition to Super fluid Turbulence

2.1. Kelvin-Helmholtz Instability in Viscous Liquids

Kelvin-Helmholtz (KH) instability is one of the many interfacial instabilities in the hydrodynamics of liquids, gases, charged plasma, and even granular materials. It refers to the dynamic instability of an interface with discontinuous tangential flow velocities and can loosely be defined as the instability of a vortex sheet. Many natural phenomena have been attributed to this instability. The most familiar ones are the generation of capillary waves on the surface of water, first analyzed by Lord Kelvin¹⁷ and the capping of sails and flags, first discussed by Lord Rayleigh¹⁸.

Many of the leading ideas in the theory of interfacial instabilities in hydrodynamics were originally inspired by considerations about ideal inviscid flow. A horizontal interface between two ideal liquids, stacked on top of each other by gravity because of their different mass densities ρ_1 and ρ_2 , and flow parallel to the interface at velocities v_1 and v_2 , leads to a convection instability at the critical differential flow velocity¹⁹

$$(v_1 - v_2)^4 = 4 \sigma (\rho_1 - \rho_2) \frac{(\rho_1 + \rho_2)^2}{\rho_1 \rho_2} : \quad (1)$$

Here σ is the surface tension of the interface and g gravitational acceleration. To separate the gravitational and inertial properties of the liquids, let us rewrite the threshold velocity in the following form

$$\frac{\rho_1 \rho_2}{\rho_1 + \rho_2} (v_1 - v_2)^2 = 2 \sqrt{\frac{\sigma}{F}} : \quad (2)$$

We associate F with the external field stabilizing the position of the interface, which in the gravitational field is the gravity force

$$F = g (\rho_1 - \rho_2) ; \quad (3)$$

but which in the general case can originate from some other source. The surface mode of ripples or capillary waves, which is first excited at the instability, has the wave number corresponding to the inverse 'capillary length',

$$k_0 = \sqrt{\frac{\sigma}{F}} : \quad (4)$$

However, ordinary fluids are not ideal and the correspondence between this theory and experiment is not good. One reason for this is that one cannot properly prepare the initial state { the shear-flow discontinuity is never in equilibrium in a viscous fluid. It is not a solution of the Navier-Stokes equation. That is why one cannot properly extend the 'instability' of the inviscid case to finite viscosities.

2.2. Kelvin-Helmholtz Instability in Superfluids

In superfluids the criterion for the instability can be formulated in the absence of viscosity, since the tangential velocity discontinuity at the interface between $^3\text{He-A}$ and $^3\text{He-B}$ is a stable non-dissipative state. These two superfluid phases have different magnetic properties and their interface is stabilized by the gradient in the applied magnetic field $H(z)$ which provides the restoring force F in Eq. (2):

$$F = \frac{1}{2} r \left(\chi_A - \chi_B \right) H^2 : \quad (5)$$

Here $\chi_A > \chi_B$ are the magnetic susceptibilities of the A and B phases, respectively. One might expect that by substituting this interfacial restoring force F into Eq. (2) and using the superfluid densities of the A and B phases instead of the total density, one obtains the critical velocity for the KH instability of the A-B interface. However, it turns out that a proper extension of the KH instability to superfluids incorporates the criterion in Eq. (2) only as a particular limiting case.

The criterion for the KH instability of ideal fluids in Eq. (2) depends only on the relative velocity across the interface. In practice there always exists a preferred reference frame, imposed by the environment. In the superfluid case it is the frame of the normal component moving with velocity v_n (in equilibrium $v_n = 0$ in a frame fixed to the rotating container). Owing to this interaction of the AB interface with its environment, the instability occurs at a lower differential flow velocity than the classical criterion in Eq. (2) assumes (see Refs. [20,15,21]):

$$\frac{1}{2} \rho_B (v_B - v_n)^2 + \frac{1}{2} \rho_A (v_A - v_n)^2 = \frac{P}{F} : \quad (6)$$

Here v_A and v_B are the velocities of the superfluid components on the A- and B-phase sides of the interface; while ρ_A and ρ_B are the corresponding densities of these superfluid fractions.

2.3. Observation of Kelvin-Helmholtz Instability

A comparison of Eq. (6) to the measured critical rotation velocity ω_c of the first KH instability event is shown in Fig. 1.²² Here we set $v_B = \omega R$ and $v_A = v_n = 0$ (i.e. the velocities are given in the frame of the rotating container, and R is the radius of the container). No fitting parameters are used. The curves have been drawn using generally accepted values for the different superfluid ^3He parameters. Even the remaining residual differences between measurement and Eq. (6) have plausible explanations which are discussed

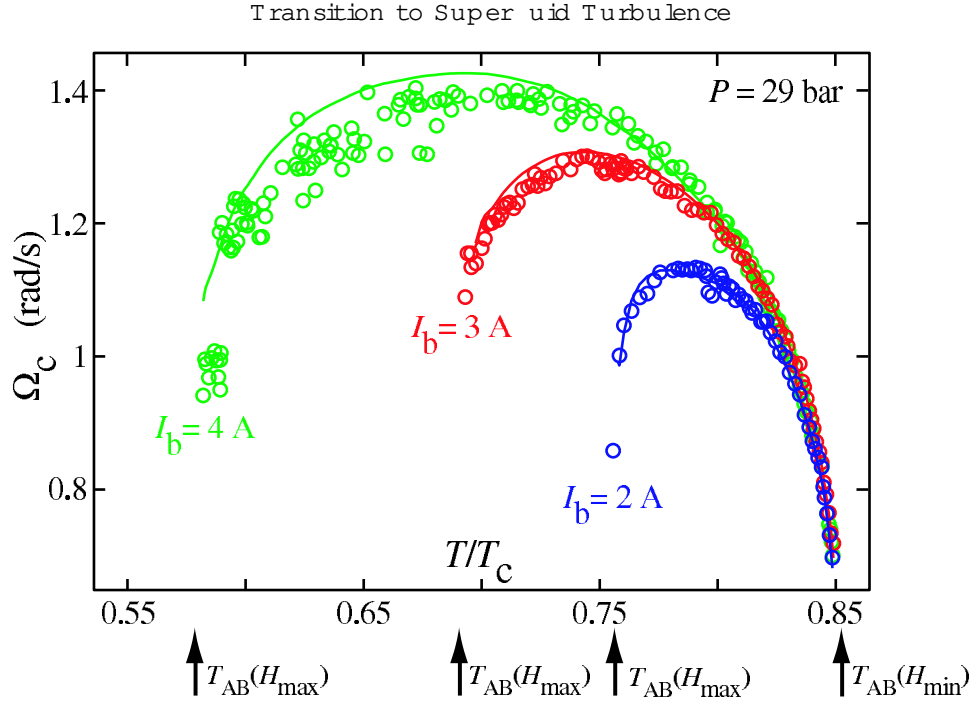


Fig. 1. Critical rotation velocity $\Omega_c = (\mathbf{v}_t - \mathbf{v}_b)/R$ of the AB-interface instability versus temperature at different currents I_b in the barrier magnet which is employed to stabilize the A phase. If the barrier field $H(z)$ exceeds the critical value $H_{AB}(T; P)$ needed for the A phase, then the AB interface resides at the two locations z where $H(z) = H_{AB}(T; P)$. These locations and the magnetic restoring force in Eq. (5) depend on temperature. The temperatures, where the AB interface disappears, are indicated by vertical arrows below the figure for different values of I_b . The solid curves represent the instability criterion (6).

in Ref. [23]. Such remarkable agreement for a complicated phenomenon can only be achieved in superfluids, where shear flow is not dissipative until the instability threshold is reached. Although the instability in Eq. (6) depends on the reference frame fixed to the normal component, this does not mean that the renormalized instability criterion would depend on the magnitude of the interaction with the normal component { in fact, it is still determined by only thermodynamics. Waves are formed on the interface when the free energy of a corrugation becomes negative in the reference frame of the environment.

In terms of the jargon accepted in general relativity, the so-called ergoregion is then formed { the region in which the (free) energy of some excitations is negative. This connection between the interface instability, horizons,

and ergoregions in black hole physics is worked out in Refs. [15,24]. In the ergoregion the AB interface becomes thermodynamically unstable, since it becomes possible to reduce the energy via the normal component and its interaction with the solid sample boundary. The original classical instability condition Eq. (2) of the ideal inviscid fluid is restored if the interaction with the environment is not effective. This might occur in the superfluid, for example, during rapid rotational acceleration at very low temperatures when the instability caused by the interaction with the environment has not had enough time to develop.

However, measurements now attest that down to moderately low temperatures of $0.35 T_c$ the instability condition is not given by the classical KH expression (2) even in a perfectly inviscid superfluid, but by the renormalized criterion in Eq. (6). Its central property is that the instability condition does not depend on the relative velocity of the two superfluids, but on the velocity of each of the superfluids with respect to the environment. The instability will occur even if the two fluids have equal densities, $\rho_A = \rho_B$, and move with the same velocity, $v_A = v_B$. The instability also occurs if there is only a single superfluid with a free surface. These new features arise from the two-fluid nature of the superfluid. The situation resembles that of a gap appearing in wind, which was originally discussed in terms of the KH instability of ideal inviscid fluids by Lord Rayleigh¹⁸. Newer explanations involve boundary interactions between the gap and the two gas streams which become turbulent within a narrow boundary layer. The superfluid analogue is an instability of a passive deformable membrane between two distinct parallel streams having the same density and velocity. The gap is the AB interface and the gap pole, which pins the gap, serves as the reference frame fixed to the environment so that Galilean invariance is violated.

2.4. Vortex Injection

The non-linear stage of the interface instability, when the interface is distorted following the break-down of its ultimate equilibrium condition, leads to the injection of a bundle of vortices from the AB interface in the rapidly flowing B-phase, when viewed in the frame of the rotating sample container. The mechanism of injection has not been worked out in detail, but a simplified scenario is presented in Fig. 2. In general, this mechanism can be associated with the non-linear development of the vortex sheet instability, as discussed e.g. in Ref. [25].

In this context the detailed properties of the injection event are not all that important. Rather we are interested in the dynamic evolution of this bundle of vortices which initially (following the instability) protrudes out of the AB interface and then continues to the cylindrical sample boundary

Transition to Super uid Turbulence

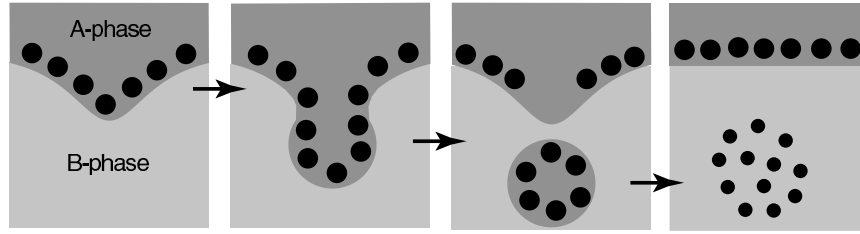


Fig. 2. One scenario for the transfer of circulation across the A-B interface in a KH instability. The A-phase vorticity is confined by the Magnus lift force to a vortex layer which covers the A-B interface.²⁶ The Magnus force arises from the tangential B-phase super flow below the interface. The instability creates a corrugation in the interface which becomes a potential well for A-phase vortices there. This pushes the vortices deeper in the potential well, deforming the corrugation to a trench with a droplet-like cross section. The trench, filled with A-phase vorticity, then propagates in the bulk B-phase where A-phase is unstable and the multiply-quantized vortex relaxes to singly-quantized B-phase vortices. In this scenario the number of vortices ejected across the interface corresponds to the number of vortices in the A-phase vortex layer within one corrugation or one half wave-length of the interface λ_{ripplon} , which is in accordance with measurements.²²

in the B-phase volume. The measurements display at first glance a rather unexpected result: The final B-phase state, i.e. the state which after some transient development will be stable in time (at constant rotation, temperature, and pressure), does not depend on the initial velocity of B-phase flow, but only on temperature.

3. SUPERFLUID TURBULENCE

3.1. Transition to Turbulence as a Function of Mutual Friction

At temperatures above $0.6T_c$ the dynamics of vortex loops injected in vortex-free flow of superfluid $^3\text{He-B}$ is regular and their number does not increase during their time-dependent evolution to rectilinear vortex lines of the rotating state. At lower temperatures it becomes possible for the vortices within a bundle of vortex loops, which is injected in a KH instability in the B-phase, to start interacting turbulently. Surprisingly this happens within a narrow temperature regime of $0.06T_c$ width centered at about $0.59T_c$, as seen in Figs. 3 and 4. The consequence from this abrupt change in the dynamics, while the vortices evolve in the externally applied flow towards

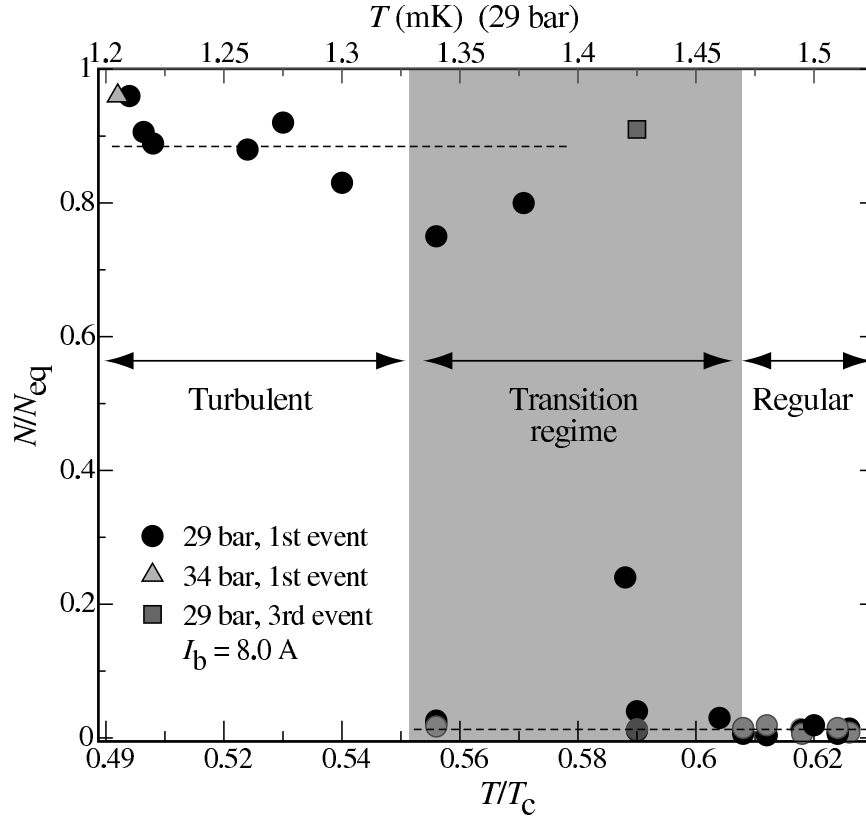


Fig. 3. Number of rectilinear B-phase vortex lines N after KH instability, normalized to the equilibrium number N_{eq} and plotted versus temperature. At around $0.58 T_c$, a sudden change in the number of lines is observed. At temperatures above the transition the injection results in only a few lines, but below the transition close to the equilibrium number is counted.

their rectilinear final state, is a radical change in the final number of vortex lines: While at temperatures above the transition the number of rectilinear vortices in the final state is a few and reproduces the distribution of vortices crossing the AB interface in one KH instability event, at temperatures below the transition the final state includes close to the equilibrium number of vortex lines.³ These properties can be examined in great detail, since the KH critical velocity stays well behaved as a function of temperature and is a continuous smooth curve across this division line, continuing to follow the calculated dependence. All this indicates that the transition is not related to the properties of the KH instability itself, but arises from the change in the dynamics of vortices moving in rapidly flowing $^3\text{He-B}$.

In Fig. 4 the phase diagram of regular and turbulent vortex dynamics is

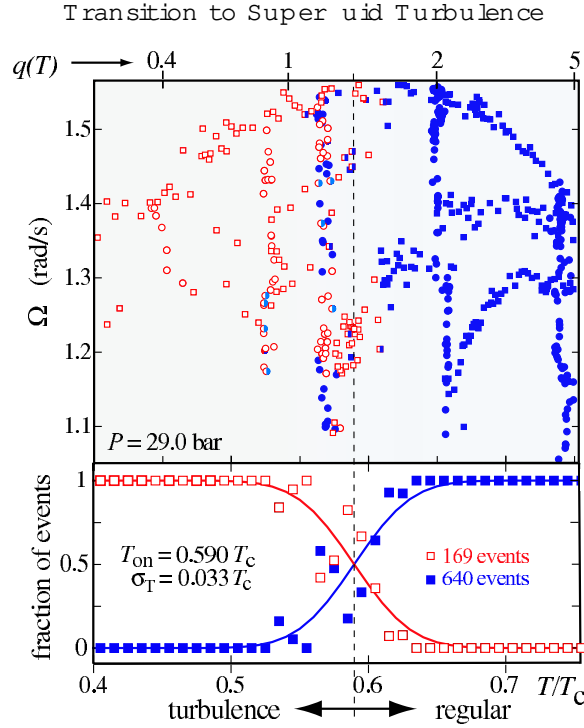


Fig. 4. Temperature { velocity phase diagram of turbulence. Each data point represents the result from a KH injection measurement where Ω is increased from zero to Ω_c at constant temperature and the number of rectilinear vortex lines N is measured in the final state. The result is marked with an open symbol, when the number is close to that in the equilibrium state N_{eq} and when turbulence must have followed injection. Regular vortex expansion with no increase in N is denoted with filled symbols. The vertical dashed line marks the boundary between the two final states. The lower plot shows the distribution of the final states in terms of gaussian fits. The horizontal top axis gives the mutual friction parameter $q(T)$.

shown as a function of flow velocity (vertical scale) and temperature (horizontal scale). The vertical axis is expressed in terms of the rotating B-phase counter flow velocity $j_B - v_n j = R$. In this diagram each data point represents a KH injection measurement, obtained with different settings of the externally controlled parameters T and I_b , so that a variation as wide as possible for the critical velocity Ω_c is obtained. What we are interested in here is the division in filled and open symbols: Injection events followed by a turbulent burst are marked with open symbols while events which lead to only a few rectilinear lines are marked with filled symbols.

The striking conclusion from Fig. 4 is that the boundary between turbulence at low temperatures and regular dynamics at high temperatures

is vertical, i.e. it is independent of the applied flow velocity above about 2.5 mm/s. It will be next shown that this transition to turbulence is driven by the dimensionless velocity independent parameter $q(T)^{-1}$, which characterizes the friction force acting on vortices when they move with respect to the normal component of the liquid. It is this parameter which divides the vortex dynamics in superfluids into a low- $l=q$ regime with regular vortex number conserving motion and a high- $l=q$ regime where superfluid turbulence becomes possible.

3.2. Superfluid Equivalent of Reynolds Number

The velocity v_L of an element of a vortex line is given by

$$v_L = v_s + \hat{s} (v_n - v_s) + \hat{s}^0 \hat{s} (v_n - v_s); \quad (7)$$

where \hat{s} is a unit vector parallel to the vortex line element. This equation of motion depends on the dimensionless mutual friction parameters (T) and $^0(T)$, which originate from the dissipative and reactive forces acting on a vortex when it moves with respect to the normal component. For vortices in a fermionic system they were calculated by Kopnin.¹⁰ For $^3\text{He-B}$ they were measured over a broad temperature range by Bevan et al.²⁷ (see also the monograph [11], where these parameters are discussed in terms of the chiral anomaly). Evidently the nature of the solutions of Eq. (7) for v_L has to depend on the mutual friction parameters.

This property will become clearer if we form the coarse-grained hydrodynamic equation for superfluid vorticity $\omega = \nabla \times v$, by averaging over vortex lines. This equation for the superfluid velocity can be obtained directly from the Euler equation for inviscid liquids where, instead of the viscous $\nu \nabla^2 v$ term of the Navier-Stokes equation, one then has (see review in Ref. [28])

$$\frac{\partial v}{\partial t} + \nabla \times v = \nabla \times (v \times v) + \nabla \times (\hat{n} \times (\hat{n} \times (v - v_n))) : \quad (8)$$

Here $v - v_n$ is the superfluid velocity, $\omega = \nabla \times v$ the superfluid vorticity, and \hat{n} the unit vector $\hat{n} = \omega/|\omega|$. In $^3\text{He-B}$ the normal component has oil-like viscosity, its motion is practically always laminar, and we ignore its dynamics. In the frame where it is at rest, i.e. $v_n = 0$, the equation for superfluid hydrodynamics is simplified:

$$\frac{\partial v}{\partial t} + \nabla \times v = (1 - ^0)\nabla \times v + \nabla \times (\hat{n} \times (\hat{n} \times v)) : \quad (9)$$

After rescaling the time, $\tau = (1 - ^0)t$, one obtains an equation which depends on a single parameter $q = ^0/(1 - ^0)$:

$$\frac{\partial v}{\partial \tau} + \nabla \times v = q \nabla \times (\hat{n} \times v) : \quad (10)$$

Transition to Superfluid Turbulence

Let us compare this equation with the Navier-Stokes equation

$$\frac{\partial \mathbf{v}}{\partial t} + \nabla \cdot (\mathbf{v} \otimes \mathbf{v}) = \nabla^2 \mathbf{v} : \quad (11)$$

The inertial terms on the lhs of Eq. (10) for superfluid hydrodynamics are the same as those on the lhs of Eq. (11) for viscous hydrodynamics. In contrast, the dissipative term on the rhs of Eq. (10) is different from the corresponding viscous term on the rhs of Eq. (11). This difference between the dissipative terms in the two equations of motion is of importance. Reynolds number, which characterizes the nature of the solutions, is formed as the dimensional equivalent of the ratio of the inertial and dissipative terms in the two hydrodynamic equations (10) and (11). For the Navier-Stokes case Eq. (11) the ratio corresponds dimensionally to the conventional Reynolds number $Re = UD/\nu$, where U is the characteristic velocity scale and D the size of the large-scale flow. In superfluid hydrodynamics Eq. (10) this ratio is simply given by the dimensionless intrinsic parameter $l=\eta$. Since $l=\eta$ does not depend on velocity or on the large-scale system size, turbulence becomes possible only if $l=\eta$ is large enough. In accordance to the usual characterization of the solutions of the Navier-Stokes equation (11) we might thus expect the transition to turbulence to occur at $l=\eta \approx 1$. This is in agreement with the experimental phase diagram in Fig. 4.

In the above considerations we used the coarse-grained description of superfluid vorticity, which does not take into account the discreteness of quantized vortices. This implies, that the flow velocity is large enough, i.e. it is essentially higher than the Feynman critical velocity, $U_c = D/\kappa$, where κ is the circulation quantum. This condition is always fulfilled in $^3\text{He-B}$ experiments, in which vortices are injected via the KH instability, since it occurs in the limit where the critical value of $l=\eta$ does not depend on the flow velocity, as seen in Fig. 4. However, at much lower velocities the critical value of $l=\eta$ is ultimately expected to increase.

Furthermore, the coarse-grained description of quantized vorticity for estimating the threshold value for $l=\eta$ assumes a sufficiently large number and density of injected vortices. The number of vortices injected in the KH instability is on average 10 (in a distribution which ranges from 3 to 30). They are packed close to each other since they originate from the same growing, but over-damped, ripplon corrugation (Fig. 2). However, in other types of injection experiments the number and density of injected vortices can be less,^{9,8} and the critical value of $l=\eta$ increases. This is similar to what occurs in viscous pipe flow⁴, where the critical Reynolds number Re for the onset of turbulence depends on the magnitude of the perturbation.

The transition from regular to turbulent dynamics as a function of the mutual friction parameter $l=\eta$ is a new phenomenon. It has not been ob-

served in $^4\text{He-II}$, where $l=q$ is practically always large, so that a transition is expected only a few tens of microkelvins below T_c where ξ is vanishingly small, the coherence length $\xi(T)$ diverges, critical velocities approach zero, and vortex dynamics enters a regime where little is known. In $^3\text{He-B}$ the transition at $l=q \approx 1$ is in the middle of the experimentally accessible temperature range and can be observed in one single experiment by scanning temperature from the superconductor-like dynamics (with no pinning, but high vortex damping) at high temperatures to superfluid ^4He -like turbulence at low temperatures.

These features demonstrate that vortex dynamics in superfluids takes varied forms and that the traditional ^4He -like behavior is just one extreme example. The opposite extreme is the strongly anisotropic superfluid $^3\text{He-A}$ where $l=q$ is practically always in the range of regular dynamics and the unusually low temperatures, which would be required for conventional superfluid turbulence, are not experimentally realistic at this time. Instead, in $^3\text{He-A}$ it is transitions in the structure of the vortex and in the global order parameter texture which provide a means to adjust to faster dynamics. An example of this is the dynamically driven transition from vortex lines to sheets in applied flow which is periodically alternating in direction³⁰ and the dependence of the critical velocity on the global order parameter texture³¹.

3.3. Turbulence in Uniform Rotation

So far measurements on the transition to turbulence have been performed in uniformly rotating flow of $^2\text{He-B}$. The long smooth-walled sample container was prepared from fused quartz with an aspect ratio (length to diameter) of almost 20. The sample can be examined in single phase configuration filled with only B phase, when the barrier magnet is not charged. In the opposite case the barrier field stabilizes over the central section of sample length a narrow layer of A phase which acts as a vortex barrier. The two end sections of equal length with B phase represent then two independent samples, whose lengths are roughly half of that of the single phase sample. In this way one can examine the influence of the length of the cylinder on the evolution and propagation of vortices in the rotating column. Another bonus is the possibility to study two B-phase samples in parallel when the A-phase barrier layer is present. This feature is of importance since the critical velocity of the sample container is an unknown predicament. The precondition for KH injection measurements is a high critical velocity. This restricts measurements to an open cylindrical volume with smooth clean walls, no internal measuring probes, and isolated from the rest of the liquid ^3He volume by a small orifice in the center of one of the flat end plates. The number of rectilinear vortices in these two B phase sections is monitored with non-

Transition to Super uid Turbulence

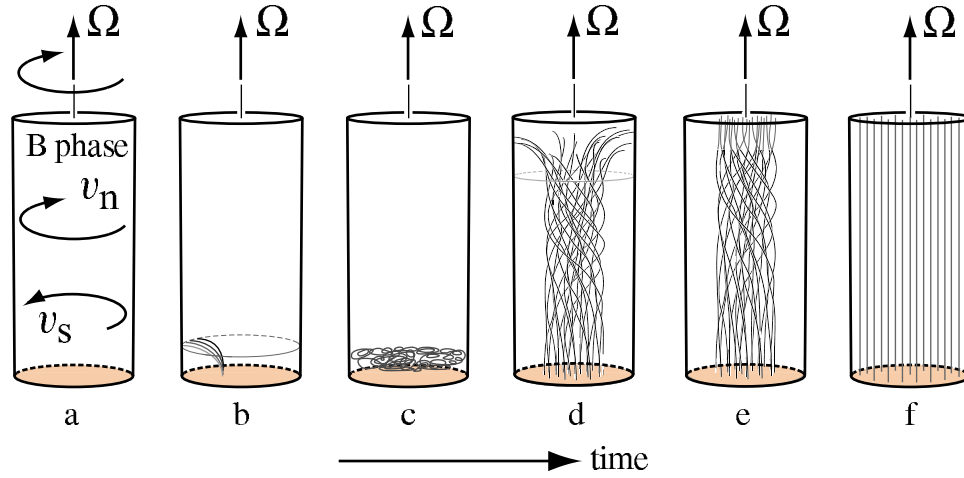


Fig. 5. Temporal evolution of vorticity in a rotating column, shown schematically (in the rotating frame) following the injection of seed vortices across the AB interface in a KH instability (at $T > 0.40 T_c$). (a) Vortex-free initial state above AB interface. (b) A tight bundle of 10 vortex loops is ejected across the AB interface in a KH instability. (c) A brief burst of turbulence spreads across the entire cross section next to the AB interface. Close to the equilibrium number of independent vortices is created and immediately polarized. (d) The vortices expand in spiral motion along the column with a sharp front towards the vortex-free section. (e) When the front reaches the top end plate, the twisted vortex state continues relaxing to rectilinear lines. If the twist is not too tight, then it is removed by the slow diffusive motion of the vortex ends on both end plates. (f) Final stable equilibrium vortex state with rectilinear lines.

invasive NMR absorption measurements, by means of NMR detector coils mounted outside around both ends of the long quartz cylinder.

Rotation provides a strong polarization for the vorticity to be oriented along the rotation axis. It is known from studies of turbulence in rotating viscous fluids that turbulent disorder then tends to become limited to the transverse plane. A similar phenomenon occurs in thermal counterflow of rotating $^4\text{He-II}$, if the thermal current is imposed parallel to the rotation axis so that it counteracts the polarization from rotation.³² Thus turbulence in effect tends to become 2-dimensional in rotation. In the case of KH injection turbulence is limited to a brief burst which takes place in the cross section of the cylinder next to the AB interface where the injection occurs. In this short burst the equilibrium number of vortices is created and, because of rapid polarization, the free energy drops instantaneously within this cross section from the maximum close to the minimum value. In Fig. 5 the ensuing

evolution of the vorticity is shown schematically. It consists of the winding cork-screw-like propagation of the vorticity along the rotating column, and the final straightening of the helically twisted vortices towards rectilinear lines of the stable equilibrium vortex state.³³

The spiralling vortex motion in the rotating column can be seen to emerge from Eq. (7). Let us write the expression for the velocity of the end point of a vortex, where it connects in perpendicular orientation to the cylindrical side wall of the sample container. In the vortex front this end point practically resides in vortex-free counterflow with $v_n = \hat{R}$ and $v_s = 0$, so that its velocity is

$$v_L = (1 - \frac{v_n}{v_s}) \hat{R} + \hat{R} \hat{z}; \quad (12)$$

which includes two components. The first component enforces azimuthal motion which differs by the fraction $1 - \frac{v_n}{v_s}$ from the velocity \hat{R} at which the superfluid component travels with respect to the cylinder wall. The second component moving with the velocity \hat{R} corresponds to the longitudinal expansion of the vortex end along the column.

With decreasing temperature the longitudinal motion slows down and ultimately becomes exceedingly slow. Since the KH instability occurs at a well-defined critical velocity, it can be started as a triggered event and the longitudinal expansion velocity can be measured by timing the time delay from the trigger to the moment when the vortex front reaches a detector coil.⁵ At higher temperatures above $0.40 T_c$ the longitudinal velocity of the front is found to be close to \hat{R} .³⁴ Thus the above scenario explains qualitatively the formation of the twisted vortex state behind the vortex front. The twisted state corresponds to dynamic equilibrium in a 'force-free configuration'.³³ This means that the residual superfluid velocity created by the twist of the vortices, which has both radial and longitudinal components, is strictly oriented along the vortex cores. With decreasing temperature the vortex front becomes sharper, the longitudinal expansion is slowed down, the twist in the trailing vortex bundle is wound ever tighter, and the residual superflow velocity along the vortices increases. Ultimately the flow along the vortices is expected to make them unstable with respect to the Glaberson-Donnelly Kelvin-wave instability and inter-vortex reconnections will become frequent behind the vortex front.³⁵ Such reconnections help to remove the twist and to speed up the relaxation of the twisted state towards the stable equilibrium vortex state with rectilinear lines (Fig. 5).

4. CONCLUSION

Although the two helium superfluids, $^4\text{He-II}$ and $^3\text{He-B}$, were expected to obey similar hydrodynamics, they differ somewhat in the actual values of

Transition to Superfluid Turbulence

their hydrodynamic properties. Rather surprisingly, these small differences have led to new insight in superfluid dynamics during recent years. An example is the transition between turbulent and regular vortex dynamics as a function of mutual friction dissipation (Γ). In the superfluid literature a 'transition to turbulence' has so far been associated exclusively with the transition in $^4\text{He-II}$ as a function of the applied flow velocity.²⁹ These velocities, at which vortices typically become mobile in $^4\text{He-II}$, are very low compared to the intrinsic critical velocity of the bulk superfluid. In contrast, the mutual friction driven transition to turbulence at high flow velocities is velocity independent. Among the various coherent quantum systems $^3\text{He-B}$ is unique in that (Γ) spans the range where $1=q = (1 - \eta^2)^{1/2}$ passes through the transition at $1=q = 1$. A similar situation might become available in atomic Bose-Einstein condensates, where mutual friction³⁶ has also been predicted to include the regime $1=q > 1$ and where turbulence might soon be experimentally realized³⁷.

A second advantage in using $^3\text{He-B}$ for vortex dynamics studies is the high viscosity of its normal component. This guarantees that the normal component is practically always in a state of laminar flow and provides a well-behaved reference frame for superfluid dynamics. This simple situation is quite unlike that in $^4\text{He-II}$, where the coupled dynamics of the superfluid and normal components have to be included from the start. Finally we note that owing to the much larger superfluid coherence length (ξ) $> 10\text{ nm}$, which determines the length scale for the radius of the vortex core in isotropic He superfluids, critical velocities can be controlled more efficiently in $^3\text{He-B}$. This allows new types of experimental studies. One example is the externally controlled introduction of seed vortices in vortex-free flow which made it possible to identify the mutual-friction-dependent transition to turbulence. The superfluid KH instability of the AB interface in a two-phase sample of ^3He superfluids is one of the unique and most reproducible of such injection methods. At present time this is the method by which a direct transition to bulk turbulence is believed to start at the lowest possible value of $1=q$.

Acknowledgements: This work is supported in part by the EU Transnational Access Programme FP6 (# RITA-CT-2003-505313), by the Academy of Finland via its 2006 grant for visitors from Russia, by the Russian Ministry of Education and Science (Leading Scientific School grant # 1157.2006.2), and by the European Science Foundation COSLAB Programme.

REFERENCES

1. R.P. Feynman, Application of quantum mechanics to liquid helium, in Prog. Low Temp. Phys., Vol. I, Ch. 2, editor C.J. Gorter (North-Holland Publ. Co., Amsterdam, 1955).

2. W.F. Vinen, Vortex lines in liquid helium II, in *Prog. Low Temp. Phys.*, Vol. III, Ch. 1, editor C.J. Gorter (North-Holland Publ. Co., Amsterdam, 1961).
3. A.P. Finne, T. Arai, R. Blaauwgeers, V.B. Eltsov, N.B. Kopnin, M. Krusius, L. Skrbek, M. Tsubota, and G.E. Volovik, *Nature*, 424, 1022 (2003).
4. B. Hof, A. Juel, and T. Mullin, Scaling of the turbulence transition threshold in a pipe, *Phys. Rev. Lett.*, 91, 24452 (2003); T. Mullin and J. Peixinho, Transition to turbulence in pipe flow, *J. Low Temp. Phys.*, this issue.
5. A.P. Finne, S. Boldarev, V.B. Eltsov, and M. Krusius, Measurement of turbulence in superfluid $^3\text{He-B}$, *J. Low Temp. Phys.*, 136, 249 (2004).
6. W.F. Vinen, An introduction to quantum turbulence, *J. Low Temp. Phys.*, this issue.
7. A.P. Finne, S. Boldarev, V.B. Eltsov, and M. Krusius, Vortex formation in neutron-irradiated rotating superfluid $^3\text{He-B}$, *J. Low Temp. Phys.* 135, 479 (2004).
8. R.E. Solntsev, R. de Graaf, V.B. Eltsov, R. Hanninen, and M. Krusius, Dynamic remnant vortices in superfluid $^3\text{He-B}$, *Proc. Quantum Fluids and Solids Conf.* 2006, *J. Low Temp. Phys.* (2007), cond-mat/0607323.
9. A.P. Finne, V.B. Eltsov, G. Eski, R. Hanninen, J. Kopu, M. Krusius, E.V. Thuneberg, and M. Tsubota, Vortex multiplication in applied flow: a precursor to superfluid turbulence, *Phys. Rev. Lett.* 96, 085301 (2006); and to be published.
10. N.B. Kopnin, *Theory of nonequilibrium superconductivity* (Clarendon Press, Oxford, 2001).
11. G.E. Volovik, *The universe in a helium droplet* (Clarendon Press, Oxford, 2003).
12. R. Combescot, Ultracold Fermi gases: the BEC-BCS crossover, *J. Low Temp. Phys.*, this issue.
13. V.S. L'vov, S.V. Nazarenko, and G.E. Volovik, Energy spectra of developed superfluid turbulence, *JETP Lett.* 80, 479 (2004); W.F. Vinen, Theory of quantum grid turbulence in superfluid $^3\text{He-B}$, *Phys. Rev. B* 71, 24513 (2005).
14. V.S. L'vov, S.V. Nazarenko, and L. Skrbek, Energy spectra of developed turbulence in helium superfluids, *J. Low Temp. Phys.*, this issue, nlin.CD/0606002.
15. G.E. Volovik, Horizons and ergoregions in superfluids, *J. Low Temp. Phys.*, this issue, gr-qc/0603093.
16. See also a more extensive review in preparation: A.P. Finne, V.B. Eltsov, R. Hanninen, N.B. Kopnin, J. Kopu, M. Krusius, M. Tsubota and G.E. Volovik, Novel hydrodynamic phenomena in superfluid ^3He , cond-mat/0606619.
17. Lord Kelvin (Sir William Thomson), *Mathematical and physical papers*, Vol. 4, Hydrodynamics and general dynamics (Cambridge University Press, 1910).
18. Lord Rayleigh (J.W. Strutt), *Scientific papers*, Vol. 1 (Cambridge University Press, 1899).
19. L.D. Landau and E.M. Lifshitz, *Fluid Mechanics* (Pergamon Press, Oxford, UK, 2nd edition, 1987).
20. G.E. Volovik, *JETP Lett.* 75, 418 (2002) and *JETP Lett.* 76, 240 (2002).
21. D.A. Abanin, *JETP Lett.* 77 191 (2003).
22. R. Blaauwgeers, V.B. Eltsov, G. Eski, A.P. Finne, R.P. Haley, M. Krusius, J.J. Ruohio, L. Skrbek, and G.E. Volovik, Shear flow and Kelvin-Helmholtz instability in superfluids, *Phys. Rev. Lett.* 89, 155301 (2002).
23. T. Ruokola and J. Kopu, Kelvin-Helmholtz instability in anisotropic superfluids

Transition to Super uid Turbulence

- ids, JETP Lett. 81, 634 (2005); and to be published.
24. R. Schutzheld and W. G. Unruh, Phys. Rev. D 66, 044019 (2002).
25. M. A. Abdal and A. Verga, Vortex sheet dynamics and turbulence, physics/0607108.
26. R. Hanninen, R. Blaauwgeers, V. B. Eltsov, A. P. Finne, M. K. Kuisius, E. V. Thuneberg, and G. E. Volvik, Structure of the surface vortex sheet between two rotating ^3He superfluids, Phys. Rev. Lett. 90, 225301 (2003).
27. T. D. C. Bevan, A. J. Manninen, J. B. Cook, H. A. Les, J. R. Hook and H. E. Hall, J. Low Temp. Phys. 109, 423 (1997).
28. E. B. Sonin, Vortex oscillations and hydrodynamics of rotating superfluids, Rev. Mod. Phys. 59, 87 (1987).
29. L. Skrbek, Flow phase diagram for the helium superfluids, JETP Lett. 80, 484 (2004).
30. V. B. Eltsov, R. Blaauwgeers, N. B. Kopnin, M. K. Kuisius, J. J. Ruohio, R. Schanzen, and E. V. Thuneberg, Transitions from vortex lines to sheets: Interplay of topology and dynamics in an anisotropic superfluid, Phys. Rev. Lett. 88, 065301 (2002).
31. V. M. H. Ruutu, J. K. Kopu, M. K. Kuisius, U. Parts, B. P. Lacaïs, E. V. Thuneberg, and W. Xu, Critical velocity of vortex nucleation in rotating superfluid $^3\text{He-A}$, Phys. Rev. Lett. 79, 5058 (1997); J. K. Kopu and E. V. Thuneberg, One-dimensional textures and critical velocity in superfluid $^3\text{He-A}$, Phys. Rev. B 62, 12374 (2000).
32. M. Tsubota, T. A. Raki, and C. F. Barenghi, Rotating superfluid turbulence, Phys. Rev. Lett. 90, 205301 (2003). Based on measurements by: C. E. Swanson, C. F. Barenghi, and R. J. Donnelly, Rotation of a tangle of quantized vortex lines in He-II, Phys. Rev. Lett. 50, 190 (1983).
33. V. B. Eltsov, A. P. Finne, R. Hanninen, J. K. Kopu, M. K. Kuisius, M. Tsubota and E. V. Thuneberg, Twisted vortex state, Phys. Rev. Lett. 96, 215302 (2006).
34. A. P. Finne, V. B. Eltsov, R. Blaauwgeers, M. K. Kuisius, Z. Janu, and L. Skrbek, Time-of-flight measurements on quantized vortex lines in rotating $^3\text{He-B}$, J. Low Temp. Phys. 134, 375 (2004).
35. R. M. O. Stern and W. J. G. Laberson, Instability of vortex lines in the presence of axial normal flow, J. Low Temp. Phys. 21, 191 (1975); Phys. Rev. Lett. 33, 1197 (1974).
36. M. Kobayashi and M. Tsubota, Thermal dissipation in quantum turbulence, cond-mat/0607434.
37. N. G. Parker and C. S. Adams, Emergence and decay of turbulence in stirred atomic Bose-Einstein condensates, Phys. Rev. Lett. 95, 145301 (2005); V. Schweikhard, I. Coddington, P. Engels, S. Tung, and E. A. Cornell, Vortex-lattice dynamics in rotating spinor Bose-Einstein condensates, Phys. Rev. Lett. 93, 210403 (2004).